Predictive Transport Simulations Consistent with Rotation and Radial Electric Field Using TOPICS with OFMC

M. Honda 1), N. Hayashi 1), T. Takizuka 2), M. Yoshida 1) and F. Fujita 1)

1) Japan Atomic Energy Agency, Naka, Ibaraki, Japan
2) Graduate School of Engineering, Osaka University, Suita, Osaka, Japan

e-mail contact of main author: honda.mitsuru@jaea.go.jp

Abstract. A toroidal momentum solver has been derived for the 1.5D integrated transport code TOPICS from the equation of motion and it calculates the evolution of the toroidal angular momentum density summed over thermal species. A novel scheme that can uniquely determine the radial electric field E_r without iterative calculations has been modeled and is also used to compute the parallel and toroidal flows for each species based on the neoclassical transport theory. The combination of TOPICS and OFMC enables us to predict the evolution of not only the density, temperature and safety factor but also the toroidal momentum and E_r. The framework developed has been tested against experiments and showed the predictive capability of toroidal rotation profile. Several time-dependent simulations in which toroidal rotation and E_r play a important role have been carried out, showing that the turbulence suppression due to the steep E_r gradient is of crucial importance in the formation of transport barriers and the direction of toroidal rotation significantly alters the confinement via the change in E_r: Co toroidal rotation gives the best performance of all in the formation of an edge transport barrier. The result qualitatively agrees with experimental observations.

1. Introduction

Toroidal rotation and its shear suppress not only directly MHD instabilities but also indirectly turbulence through a variation of a radial electric field E_r in that the radial force balance equation essentially determines E_r in conjunction with a pressure gradient, poloidal and toroidal flows. Computing the evolution of a whole plasma comprehensively, a transport code has to be capable of tracking the evolution of toroidal rotation and E_r as well as density and temperature. Nonetheless, a solver of the toroidal momentum that governs toroidal rotation has not been widely implemented in transport codes from the standpoint of a self-consistent coupling with E_r, or has not been extensively exploited for predicting a plasma evolution and developing an operation scenario thus far even if it has been implemented anyhow. This is partly because the subject of toroidal momentum transport has been less understood compared to that of particle and heat transport. Recently, from the aspect of both theories and experiments, toroidal momentum transport is being understood [1] and several momentum transport models have been proposed, being able to be implemented in a transport code. It is feasible to accurately estimate E_r in transport simulations only when a toroidal momentum equation is solved. Based on the fact that E_r and its shear play an important role in the turbulence suppression, the orbit squeezing for thermal particles, the neoclassical toroidal viscosity, the intrinsic torque source due to symmetry breaking and so on, a toroidal momentum solver makes itself indispensable to transport simulations.

The 1.5D integrated transport code TOPICS (see e.g. [2]) developed in JAEA has not yet incorporated a toroidal momentum solver and thus computed E_r solely by the pressure gradient as needed. This time we derive not an intuitive, but a solid toroidal momentum equation with imposed assumptions clarified in the course of derivation, starting from an equation of motion. At the same time, we develop a scheme that uniquely determining E_r without iterations: in general a convergence loop is required because several quantities affecting E_r depend upon E_r [3]. In current experiments toroidal rotation is mainly driven by directional neutral beam (NB) injection as an external torque input. In the TOPICS framework, based on an equilibrium computed by TOPICS, the fast-ion Orbit-Following Monte Carlo (OFMC) code calculates the

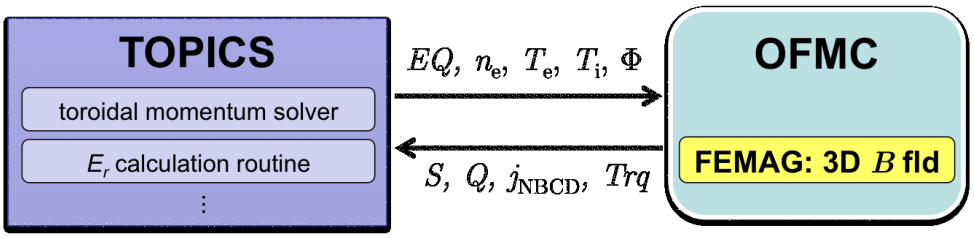

FIG. 1. Schematic diagram of the close coupling of TOPICS and OFMC.

collisional and $\boldsymbol{j} \times \boldsymbol{B}$ torques as well as the particle and heat sources and the driven current, all of which are thus transferred to TOPICS, as schematically viewed in figure 1.

The framework newly developed realizes transport simulations in which the density, temperature, safety factor, toroidal momentum and equilibrium are all consistent with each other. Most of the quantities are more or less linked via E_r. With the aid of appropriate transport models, TOPICS now can firmly tackle the problems in which E_r does play a crucial role, such as the formation of internal and edge transport barriers. In this paper, we describe details of the modelings and subsequently show simulation results that are possible to be shown using the novel framework for the first time.

2. Modeling Equations for Toroidal Momentum and E_r

2.1. Toroidal Momentum Equation

In an axisymmetric system, toroidal angular momentum is conserved to the 1st order in $\delta \equiv \rho_L/L \ll 1$, where ρ_L is the Larmor radius and L the characteristic length, and radial transport of toroidal angular momentum is effective to the 2nd order. We therefore maintain terms up to $O(\delta^2)$ when we derive a governing equation of toroidal angular momentum. We postulate that we take account of total toroidal angular momentum density summed over thermal species (the toroidal momentum, hereafter), because thanks to the summation its governing equation does not include the friction forces between thermal species and does explicitly include the $\boldsymbol{j} \times \boldsymbol{B}$ term from the Lorentz force term, which can be subsequently replaced by the fast-ion $\boldsymbol{j} \times \boldsymbol{B}$ torque computed by OFMC.

Starting from an equation of motion in the conservative form, we take the toroidal projection, $R^2\nabla\phi$, and take the sum over thermal species to obtain

$$\frac{\partial}{\partial t}(mnRV_\phi)\bigg|_{\boldsymbol{x}} + \nabla\cdot\left(\sum_s m_s n_s R V_{s\phi}\boldsymbol{V}_s\right) = \sum_s\left(-R^2\nabla\phi\cdot\nabla\cdot\overleftrightarrow{\pi}_s + e_s n_s R^2\nabla\phi\cdot\boldsymbol{V}_s\times\boldsymbol{B} + R\bar{S}_{ms\phi}\right) - \sum_{j=\mathrm{fast}} e_j n_j R^2\nabla\phi\cdot\boldsymbol{E},$$

where the subscript s denotes thermal species including electrons, $\bar{S}_{m\phi}$ the momentum source, say collisional torque due to NBI, and the other notation is standard. Note that the deceleration term by the toroidal electric field remains due to the quasineutrality condition, $0 = \sum_{k=\mathrm{all}} Z_k n_k = \sum_s Z_s n_s + \sum_{j=\mathrm{fast}} Z_j n_j$. Transforming the coordinates from the laboratory frame $\boldsymbol{x}$ to the moving frame and taking the flux-surface average, we have

$$\frac{1}{V'}\frac{\partial}{\partial t}(V'\langle\mathcal{L}\rangle)\bigg|_\rho + \frac{1}{V'}\frac{\partial}{\partial\rho}\left[V'\sum_s m_s\langle RV_{s\phi}\rangle\Gamma_s\right] = -\sum_s\langle R^2\nabla\phi\cdot\nabla\cdot\overleftrightarrow{\pi}_s\rangle - \langle\boldsymbol{j}_\mathrm{b}\cdot\nabla\psi\rangle + \sum_s\langle R\bar{S}_{ms\phi}\rangle - \sum_{j=\mathrm{fast}} e_j n_{j0}\langle RE^A_\phi\rangle, \quad (1)$$

where the subscript 0 denotes the flux function, $\langle\mathcal{L}\rangle \equiv \sum_s m_s n_{s0}\langle RV_{s\phi}\rangle$ and $\Gamma_s \simeq n_{s0}\langle(\boldsymbol{V}_s - \boldsymbol{u}_g)\cdot\nabla\rho\rangle$. Due to the large neoclassical dielectric constant of a plasma, $\langle\boldsymbol{j}\cdot\nabla\psi\rangle \simeq -\langle\boldsymbol{j}_{\rm b}\cdot\nabla\psi\rangle$. The lowest-order viscosity tensor has the Chew-Goldberger-Low (CGL) form, which vanishes due to axisymmetry. To the next order the turbulent viscosity becomes dominant and is described by the spatial gradient of a momentum flux, which is modeled by the sum of the momentum convection (inward pinch), the momentum diffusion and the residual stress [4]. Unlike particle and heat, the momentum pinch is typically always inward and is related to the momentum diffusivity χ_ϕ [5, 6, 7]. Since the neoclassical momentum diffusivity is negligibly small [8, 9], χ_ϕ is considered to be purely turbulent. Typically we assume $\chi_\phi = {\rm Pr}\chi_{\rm i}^{\rm turb}$ using the Prandtl number Pr. The residual stress is independent of toroidal velocity and is thus possible to drive toroidal rotation from rest [4]. In TOPICS, only an $\boldsymbol{E}\times\boldsymbol{B}$ flow shear contribution is modeled [10] among other sources like up-down asymmetry and turbulence intensity gradient. The current residual-stress model is proportional to χ_ϕ as well. Let us now consider how large a contribution of a momentum diffusive flux of each species to a total diffusion flux is in a plasma comprised of electron, deuterium and carbon, for example. Then we reasonably speculate $n_{\rm e} \sim n_{\rm D} > n_{\rm C}$, $V_{{\rm e}\phi} \sim V_{{\rm D}\phi} \sim V_{{\rm C}\phi}$, $m_{\rm e} \ll m_{\rm D} < m_{\rm C}$, resulting in $\sum_s \chi_{s\phi}\partial_\rho\langle\mathcal{L}_s\rangle \approx \chi_\phi\partial_\rho\langle\mathcal{L}\rangle$, where a common χ_ϕ is estimated by bulk ions'. This is also the case with the momentum pinch. This process diagonalizes Eq. (1) with respect to $\langle\mathcal{L}\rangle$. Consequently, we have the final form of the toroidal momentum equation as follows:

$$\frac{1}{V'}\frac{\partial}{\partial t}(V'\langle\mathcal{L}\rangle)\bigg|_\rho = -\frac{1}{V'}\frac{\partial}{\partial\rho}V'\bigg[\langle|\nabla\rho|\rangle\nu\langle\mathcal{L}\rangle - \langle|\nabla\rho|^2\rangle\chi_\phi\frac{\partial\langle\mathcal{L}\rangle}{\partial\rho} + \langle|\nabla\rho|\rangle\sum_s\Gamma_s m_s\langle RV_{s\phi}\rangle$$
$$+ \langle|\nabla\rho|^2\rangle\chi_\phi\sum_s m_s\langle RV_{s\phi}\rangle\frac{\partial n_{s0}}{\partial\rho} + \sum_s\langle\Pi_s^{\rm res}\rangle\bigg] - \langle\boldsymbol{j}_{\rm b}\cdot\nabla\psi\rangle + \sum_s\langle R\bar{S}_{ms\phi}\rangle - \sum_{j=\rm fast} e_j n_{j0}\langle RE_\phi^A\rangle. \quad (2)$$

Note that χ_ϕ influences not only the diffusive flux but also the pinch and the residual stress in the models currently used. We thus have to keep in mind that a slight change in χ_ϕ may significantly alter a profile of the toroidal momentum.

2.2. An Equation that Uniquely Determines E_r

A scheme has to be developed calculating E_r using the total toroidal momentum $\langle\mathcal{L}\rangle$ that is computed by solving Eq. (2). E_r can be essentially determined by the radial force balance equation consisting of ∇p, the toroidal flow and the parallel (or poloidal) flow for any thermal species. A steady-state solution of the parallel momentum equation, $\hat{L}\boldsymbol{U}_\parallel = \hat{M}[\boldsymbol{U}_\parallel - \boldsymbol{V}] - \boldsymbol{S} - \boldsymbol{E}$, gives the parallel flow in a neoclassical fashion and the equation contains the neoclassical viscous term proportional to the poloidal flow that can be rewritten by the parallel and diamagnetic flows [11]. Here, $\hat{L}$ and $\hat{M}$ denote the friction and neoclassical viscosity matrices, $\boldsymbol{V}$ the diamagnetic flow, $\boldsymbol{S}$ the parallel momentum source and $\boldsymbol{E}$ the parallel electric field. More details are given in [11]. Thus the diamagnetic flow is required for solving this equation, but it explicitly depends upon E_r. In order to avoid iterative computation to calculate E_r, we will derive a parallel flow equation explicitly including the electrostatic potential Φ by extracting terms related to Φ.

Solving the parallel momentum equation with respect to $\boldsymbol{U}_\parallel$ yields $\boldsymbol{U}_\parallel = (\hat{M}-\hat{L})^{-1}\hat{M}\boldsymbol{V} + (\hat{M}-\hat{L})^{-1}(\boldsymbol{S}+\boldsymbol{E})$, where $\boldsymbol{V}$ includes Φ. Therefore, we write $\boldsymbol{U}_\parallel$ as follows:

$$\langle BV_{s\parallel}\rangle = \sum_b\begin{pmatrix}\alpha_{sb} & \alpha_{s,b+smax}\end{pmatrix}\begin{pmatrix}\langle BV_{1b}\rangle\\ \langle BV_{2b}\rangle\end{pmatrix} + \sum_b\begin{pmatrix}\beta_{sb} & \beta_{s,b+smax}\end{pmatrix}\begin{pmatrix}e_b n_b\langle BE_\parallel\rangle + \langle BS_{mb\parallel}\rangle\\ \langle BQ_{mb\parallel}\rangle\end{pmatrix}$$
$$= I\sum_b\left[-\alpha_{sb}\left(\frac{d\Phi}{d\psi} + \frac{1}{e_b n_b}\frac{dp_b}{d\psi}\right) - \alpha_{s,b+smax}\frac{1}{e_b}\frac{dT_b}{d\psi}\right]$$

$$+\sum_b [\beta_{sb} e_b n_b \langle BE_{\|}\rangle + (\beta_{sb}\langle BS_{mb\|}\rangle + \beta_{s,b+smax}\langle BQ_{mb\|}\rangle)], \quad (3)$$

explicitly including Φ, where $\alpha_{ij} \equiv [(\hat{M}-\hat{L})^{-1}\hat{M}]_{ij}$ and $\beta_{ij} \equiv [(\hat{M}-\hat{L})^{-1}]_{ij}$, b denotes thermal species and *smax* the maximum number of the species. The α_{ij} and β_{ij} coefficients can be numerically computed by the Matrix Inversion method [11]. On the other hand, the toroidal flow is linked to the parallel and diamagnetic flows via the relationship of the first-order incompressible flow within a flux surface: $\langle RV_{s\phi}\rangle = (I/\langle B^2\rangle)\langle BV_{s\|}\rangle - (d_\psi\Phi + d_\psi p_s/(e_s n_s))(\langle R^2\rangle - I^2/\langle B^2\rangle)$. Looking at both this equation and Eq. (3), we find that substituting the latter equation to the former $d_\psi\Phi$ can be described by the known quantities. Summing the resultant equation multiplied by the mass density over thermal species to convert the toroidal flow for each species to the total toroidal momentum density, we finally have

$$\frac{d\Phi}{d\rho} = \left(\sum_s m_s n_s \sum_b \alpha^*_{sb}\right)^{-1}\left[-\frac{\langle B^2\rangle}{I^2}\frac{d\psi}{d\rho}\langle\mathcal{L}\rangle + \sum_s m_s n_s \sum_b\left(-\alpha^*_{sb}\frac{1}{e_b n_b}\frac{dp_b}{d\rho} - \alpha_{s,b+smax}\frac{1}{e_b}\frac{dT_b}{d\rho}\right)\right.$$
$$\left. + \frac{1}{I}\frac{d\psi}{d\rho}\sum_s m_s n_s \sum_b \{\beta_{sb} e_b n_b\langle BE_{\|}\rangle + (\beta_{sb}\langle BS_{mb\|}\rangle + \beta_{s,b+smax}\langle BQ_{mb\|}\rangle)\}\right], \quad (4)$$

where $\alpha^*_{sb} \equiv \alpha_{sb} + (\langle B^2\rangle\langle R^2\rangle/I^2 - 1)\delta_{sb}$. This equation can be readily solved once $\langle\mathcal{L}\rangle$, the thermodynamic forces and the sources are known. Finally, $\langle E_r\rangle \equiv -\langle\nabla\Phi\cdot\nabla r\rangle = -\langle|\nabla\rho|^2\rangle d_\rho r\, d_\rho\Phi$.

Once $d_\rho\Phi$ is resolved, the parallel flow $\langle BV_{s\|}\rangle$ for each species can be determined by virtue of Eq. (3), resulting in $\langle RV_{s\phi}\rangle$ via the incompressible flow equation. Successively determined are the rotation frequency $\langle V_{s\phi}/R\rangle$ and the flux-surface averaged toroidal rotation velocity defined by the poloidal cross section rather than the volume, $\langle V_{s\phi}\rangle_S \equiv \langle V_{s\phi}/R\rangle/\langle 1/R\rangle$. This scheme can derive such quantities for each species from $\langle\mathcal{L}\rangle$, making use of the feature that the radial force balance equation determining $d_\rho\Phi$ is valid for any species.

2.3. Validation of the Framework Developed

It is beneficial to examine whether the solver and the scheme function before predictive simulations. Different toroidal rotation profiles have been obtained in two almost equivalent JT-60U L-mode discharges, despite nearly the same torque depositions [12]. The discrepancy between them seems to just originate from the different toroidal rotation velocities at the plasma surface. In simulations, we solely solve the toroidal momentum solver and retrieve measured density, temperature and current profiles and equilibria. χ_ϕ is assumed to be $\chi_\phi = \mathrm{Pr}\chi_\mathrm{i}$, where χ_i's are

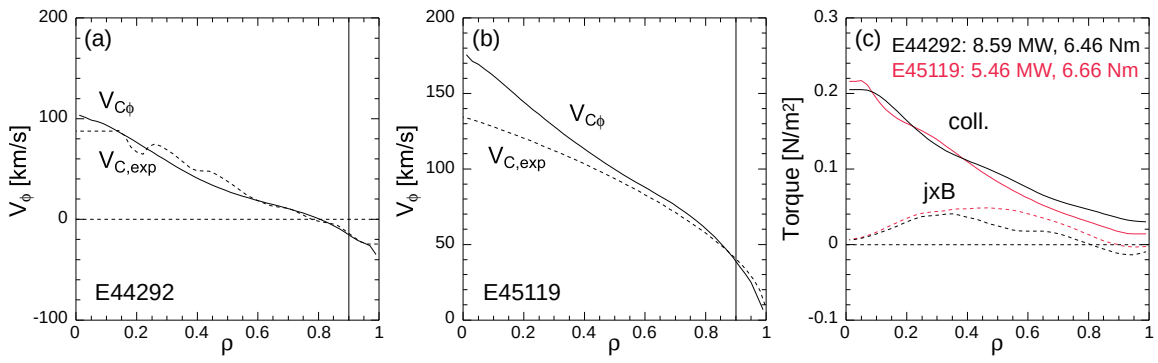

FIG. 2. Measured (dotted) and predicted (solid) carbon toroidal rotation profiles for two discharges (a) and (b). The boundary is set at $\rho = 0.9$ and its value is set to the measured one. (c) Collisional (solid) and the $\boldsymbol{j}\times\boldsymbol{B}$ (dotted) torque profiles.

taken from experimentally-analyzed profiles and Pr's of 0.6 ∼ 0.8 are given so that χ_ϕ profiles are almost equivalent to each other. The empirical pinch model is used [7] and the torque is computed by OFMC. Figure 2 shows the measured and predicted carbon toroidal rotation profiles for two discharges and the collisional and $\boldsymbol{j} \times \boldsymbol{B}$ torque profiles. The predicted profiles are fairly in good agreement with experiments, implying that the current framework has the predictive capability of toroidal rotation profiles when the appropriate χ_ϕ and the boundary conditions for $\langle \mathcal{L} \rangle$ are given. Note that due to an inward pinch, the rotation velocity at the boundary may readily change that in the core region. In this sense, how good we can predict toroidal rotation depends upon how correct we can estimate χ_ϕ and boundary values and this is an open issue.

3. The Role of Toroidal Rotation in the formation of E_r and ITBs

It has already been known in experiments that the direction of toroidal rotation influences performance of ITBs, i.e. ∇T [13]. In such plasmas, the steep ∇p locally creates a notched structure of E_r in the vicinity of an ITB, while toroidal rotation globally affects the structure and the sign. Self-consistent treatment of both E_r and toroidal rotation therefore has to be required in transport simulations especially with ITBs formed at least when a directional NB is employed.

Carrying out a simulation of the ITB formation, we prepare for a JT-60U like weakly-reversed-shear plasma with $R = 3.42\,\mathrm{m}$, $a = 0.934\,\mathrm{m}$, $B_T = 3.16\,\mathrm{T}$ and $\bar{n}_\mathrm{e} = 1.78 \times 10^{19}\,\mathrm{m}^{-3}$. The application of 4 MW near-perpendicular NBs and 4 MW co-tangential NBs commences at the beginning of a flat-top phase. In TOPICS simulations, the pressure, safety factor and equilibrium are time-dependently solved, but the density is fixed. The heat diffusivity is estimated by the CDBM model with the E_r shear stabilization effect [14] and Pr = 1 is assumed for the sake of simplicity. The minimum value of χ_ϕ of $0.5\,\mathrm{m}^2/\mathrm{s}$ is prescribed avoiding zero near the axis. The Hahm's pinch model is employed [6]. Then, we compare two cases, either using Eq. (4) for the estimate of E_r or simply using the pressure gradient solely: We call them case (1) and (2), respectively, hereafter.

Simulation results are exhibited in figure 3. Actually in both cases heat transport is greatly reduced at q_min where the magnetic shear passes through zero, irrespective of the E_r shear effect, and the ITB commences being formed, as shown in figure 3 (c) and (d). Figure 3 (b) displays, in contrast, the positive E_r solely for case (1) (red lines in the figures). On the other hand, the steep negative E_r shear appears in case (2) due solely to ∇p. Co toroidal rotation, as observed in

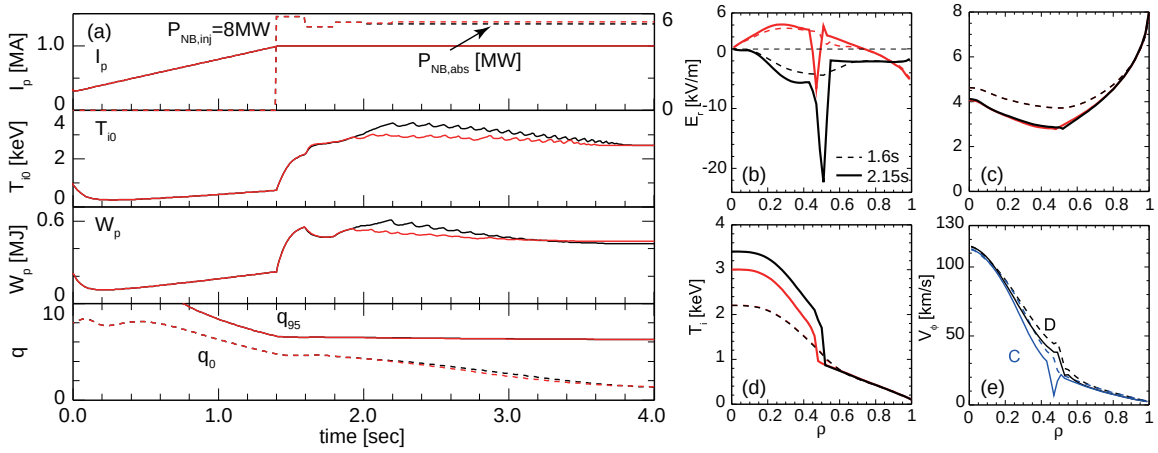

FIG. 3. (a) Time histories of the plasma current I_p, the NB absorption power P_abs, the ion temperature on axis $T_{\mathrm{i}0}$, the stored energy W_p, the safety factor on axis q_0 and at the 95% flux surface q_{95}. Red and black lines correspond to the cases using Eq. (4) and $E_r = -d_r p_\mathrm{i}/(Z_\mathrm{i} e n_\mathrm{i})$, respectively. At $t = 1.6\,\mathrm{s}$ (broken) and 2.15 s (solid), shown are the profiles of (b) E_r, (c) q, (d) the ion temperature T_i and (e) the deuterium and carbon toroidal velocities $V_{\mathrm{D}\phi}$ (black) and $V_{\mathrm{C}\phi}$ (blue) only for the case using Eq. (4).

figure 3 (e), pushes E_r into positive and tends to weaken the E_r shear because the contribution of co rotation to E_r is opposite to that of ∇p which is generally negative. For this reason, the ITB for case (2) is eventually stronger than that for case (1) and the stored energy W_p shows a sharp increase solely for case (2). The increase in temperatures inside the ITB defers the current penetration to the core especially for case (2), but in the end the weakly negative shear and thus the ITB vanish by $t = 4.0\,\mathrm{s}$ for both cases. The simulations tell us that rotation due to unidirectional NBs has to be taken into account; otherwise performance of a plasma would be readily mispredicted, regardless of a choice of a turbulent transport model.

4. Toroidal Rotation Effect on the ETB formation

It is widely believed that E_r in conjunction with toroidal rotation plays an important role at the formation of an edge transport barrier (ETB), i.e., a pedestal. While a limit of the pedestal height is bounded by peeling-ballooning instabilities, the transition itself seems to be provoked by the suppression of turbulence due mainly to the E_r shear. In the JT-60U experiments the better confinement is observed in the case with co NB injection, i.e. co toroidal rotation, compared to the case with counter or balanced injection [15]. It is the evidence that toroidal rotation is strongly linked to pedestal performance.

Several theoretical models have been proposed to give rise to L-H transition. One of the most potent mechanisms is the turbulence stabilization due to the $\boldsymbol{E}\times\boldsymbol{B}$ shear flow that depends upon E_r [16]. Nonetheless, artificial reduction in turbulent $\chi_\mathrm{e,i}$ to the neoclassical transport level prevails for transport simulations with regard to L-H transition thus far. That means that the reduction can be provoked whenever one wants L-H transition, irrespective of P_NB, E_r or even transport. Recently, transport simulations have been made to obtain the transition using an $\boldsymbol{E}\times\boldsymbol{B}$ shearing model [17, 18]. The simulation given in [17] shows that the tuned CDBM model implemented in TOPICS enables L-H transition by auxiliary heating. However, at that time the heating profiles were artificially prescribed, E_r was simply estimated solely by ∇p and toroidal rotation were neither solved nor taken into account. Now the current scheme enables us to examine the effects of toroidal rotation on E_r and performance of the ETB.

The tuned CDBM model [17] is very similar to the original one in essence. It has slightly different dependence on $s-\alpha$ and exploits the definition of the normalized ∇p, $\alpha = -q_\mathrm{eng}^2 R d_r\beta$, where $q_\mathrm{eng} \equiv 2\pi\kappa r^2 B_T/[\mu_0 R I_p(r)]$: This definition can avoid a sharp increase in α at the separatrix. The suppression due to the $\boldsymbol{E}\times\boldsymbol{B}$ shearing rate $\omega_\mathrm{E\times B}$ is expressed by the Lorentzian form and its efficacy depends upon the cube of the ratio of $\omega_\mathrm{E\times B}$ to γ_CDBM. Two arbitrary coefficients are determined by the experimental scalings. Further details are found in [17].

For simulations, a JT-60SA plasma is focused, where $R = 2.96\,\mathrm{m}$, $a = 1.133\,\mathrm{m}$, $I_\mathrm{p} = 4\,\mathrm{MA}$ and $B_T = 2.3\,\mathrm{T}$. At $t = 3.0\,\mathrm{s}$, near-perp. NB units of 2 MW each are applied. At the same time, 4 MW co-tangential NBs for the co case, 4 MW ctr-tangential NB for the ctr. case and co- and ctr-tang of 2 MW each for the balanced-injection case are also applied. The ripple effects are not considered so as to retain the nearly identical absorption power for three cases. The q and equilibrium evolution are not solved, whereas the density, pressure and toroidal momentum solvers are time-dependently computed. Pr = 1 and the Hahm's pinch model [6] are used.

As shown in figure 4 (a), the NB heating power increases from 1 MW to 8 MW at $t = 3.0\,\mathrm{s}$ and the absorption power is around 7.5 MW for each case. Before the beginning of 8 MW heating, the density in the edge gradually develops by virtue of recycling. Due to the strong NB heating the density and temperature rapidly build up almost over the entire profile, while the steep E_r gradient near the separatrix maintains transport at the low level due to the $\boldsymbol{E}\times\boldsymbol{B}$ shear flow suppression. It therefore leads to the formation of the ETB. Co rapid toroidal rotation makes E_r positive and the height of the E_r "cliff" becomes higher, leading to the further suppression of turbulence, as shown in figure 5. For the bal. case, even though E_r does not vary over

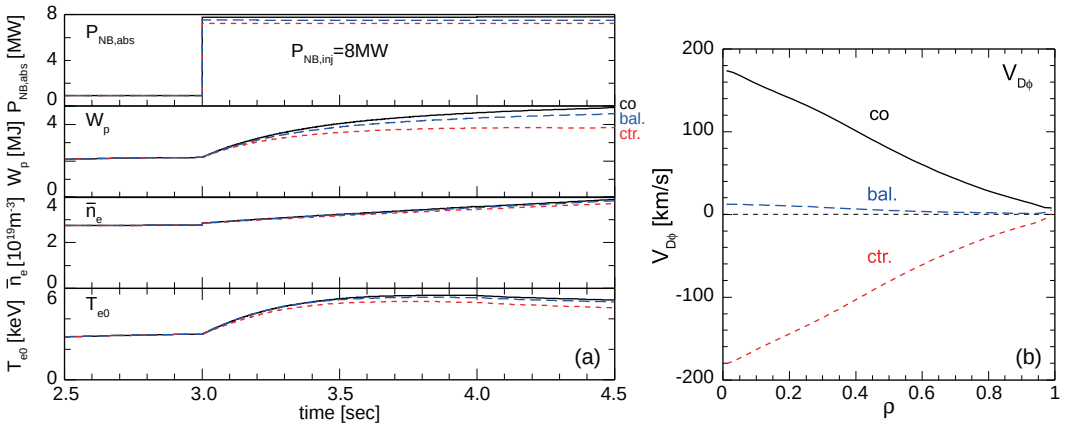

FIG. 4. (a) Time histories of $P_{\rm abs}$, $W_{\rm p}$, the line-averaged electron density $\bar{n}_{\rm e}$ and $T_{\rm i0}$. Black, red and blue lines correspond to the co, ctr. and bal. NB injection cases, respectively. (b) The toroidal rotation profiles of deuterium for three cases at t = 4.0 s.

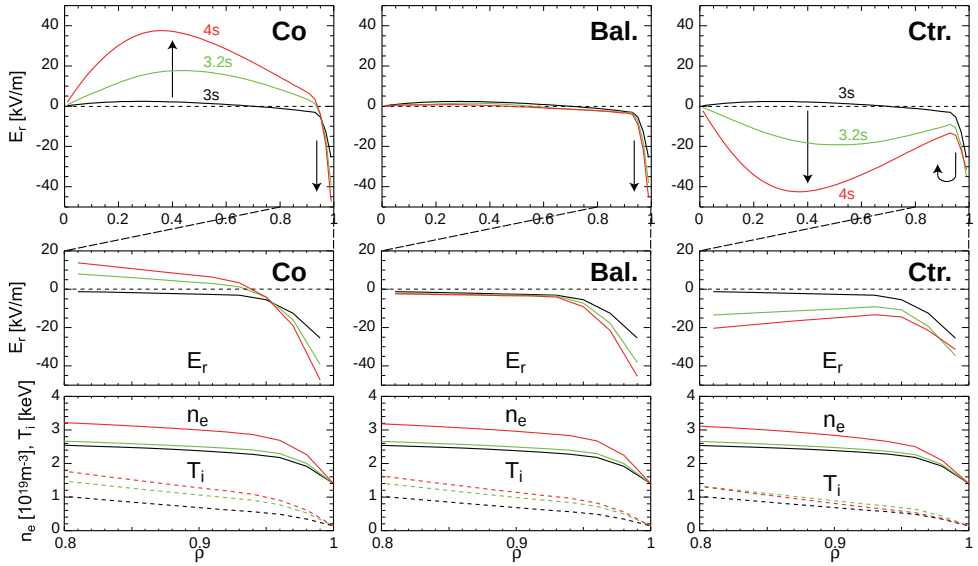

FIG. 5. The evolution of E_r profiles (top figures), magnified profiles of E_r (middle) and $n_{\rm e}$ and $T_{\rm i}$ (bottom) at t =3.0, 3.2 and 4.0 s for the co, bal. and ctr. cases.

time, its structure outside $\rho \approx 0.93$ is almost identical to that for the co case, leading to the similar pedestal for both cases. Looking carefully at E_r at the pedestal, the region of the steep E_r gradient and the subsequent reduced transport is wider for the co case than that for the bal. case due to the increase in positive E_r. Co NBI therefore leads to the better confinement. In contrast, ctr. NBI, i.e., counter toroidal rotation, produces the negative E_r analogous to the ∇p contribution, weakening the steep E_r gradient in the edge and deteriorating the confinement improvement. In our case, ctr. NBI once triggers L-H transition, but after a while the pedestal of temperature vanishes as the height of the steep E_r gradient decreases.

5. Conclusions and Discussion

The toroidal momentum solver has been derived for TOPICS from the equation of motion and it calculates the evolution of the toroidal angular momentum density summed over thermal species, $\langle \mathcal{L} \rangle$. The novel scheme that can uniquely determine E_r using $\langle \mathcal{L} \rangle$ without iterative calculations has been modeled. Those have been successfully implemented into TOPICS. The combination of TOPICS and OFMC enables us to predict the evolution of not only the density,

temperature and q but also the toroidal momentum and E_r self-consistently. With the aid of the Matrix Inversion method, the parallel and toroidal flows can be computed for each species based on the neoclassical transport theory.

The simulations of the toroidal rotation evolution show that predicted toroidal rotation profiles are in good agreement with experimental observations for two JT-60U discharges with different boundary values, once the measured profiles and the appropriate boundary condition are provided. They demonstrates the validity of the framework developed.

We have paid attention to the time-dependent simulations in which toroidal rotation and E_r play a crucial role, i.e. the ITB and ETB formation. Even though results may differ depending on what turbulent transport models are chosen, the turbulence suppression due to the $\boldsymbol{E} \times \boldsymbol{B}$ flow shear is required or, to say at least, important to provoke transition. The fact manifests the necessity of accurately calculating E_r in transport simulations. In this sense, predicting toroidal rotation is indispensable because toroidal rotation is virtually a unique player that can change sign in E_r. In fact, our simulations of the ETB formation clearly display that co toroidal rotation facilitates achieving the better confinement through the change in the E_r structure, unlike nearly zero or counter rotation. These results indicate that it is vital to predict toroidal rotation and E_r for transport simulations and development of operation scenarios.

The authors would like to express their sincere gratitude to Drs. S. Ide, K. Shinohara, H. Urano, M. Yagi and Y. Kosuga for fruitful discussion and to Messrs. I. Kamata and M. Suzuki for numerical assistance. This work was supported by a Grant-in-Aid for Young Scientists (B) (No 22760667) from the Japan Society for the Promotion of Science (JSPS) and was carried out using the HELIOS supercomputer system at International Fusion Energy Research Centre, Aomori, Japan, under the Broader Approach collaboration between Euratom and Japan, implemented by Fusion for Energy and JAEA

References

[1] PEETERS, A.G., et al., Nucl. Fusion **51** (2011) 094027.
[2] HONDA, M., Comput. Phys. Commun. **181** (2010) 1490.
[3] ARTAUD, J.F., et al., Nucl. Fusion **50** (2010) 043001.
[4] DIAMOND, P.H., et al., Nucl. Fusion **49** (2009) 045002.
[5] PEETERS, A., ANGIONI, C., STRINTZI, D., Phys. Rev. Lett. **98** (2007) 265003.
PEETERS, A., et al., Phys. Plasmas **16** (2009) 062311.
[6] HAHM, T.S., et al., Phys. Plasmas **14** (2007) 072302.
[7] TALA, T., et al., Nucl. Fusion **51** (2011) 123002.
[8] HINTON, H.L., WONG, S.K., Phys. Fluids **28** (1985) 3082.
[9] NISHIJIMA, D., et al., Plasma Phys. Control. Fusion **47** (2005) 89.
[10] KOSUGA, Y., DIAMOND, P.H., GÜRCAN, Ö.D., Phys. Plasmas **17** (2010) 102313.
[11] KIKUCHI, M., AZUMI, M., Plasma Phys. Control. Fusion **37** (1995) 1215.
[12] YOSHIDA, M., et al., Plasma Phys. Control. Fusion **48** (2006) 1673.
[13] SAKAMOTO, Y., et al., Nucl. Fusion **41** (2001) 865.
[14] FUKUYAMA, A., et al., Plasma Phys. Control. Fusion **38** (1996) 1319.
[15] URANO, H., et al., Nucl. Fusion **48** (2008) 085007.
[16] BURRELL, K.H., Phys. Plasmas **4** (1997) 1499.
[17] YAGI, M., et al., Contrib. Plasma Phys. **52** (2012) 372.
[18] PIANROJ, Y., TECHAKUNCHAIYANUNT, J., ONJUN, T., J. Phys. Soc. Jpn. **81** (2012) 044502.